ELSEVIER

Ceramics International 31 (2005) 525–531

CERAMICS INTERNATIONAL

www.elsevier.com/locate/ceramint

# Effects of SiC sub-layer on mechanical properties of Tyranno-SA/SiC composites with multiple interlayers

Wen Yang[a,*], Hiroshi Araki[a], Akira Kohyama[b], Hiroshi Suzuki[a], Tetsuji Noda[a]

[a]*National Institute for Materials Science, Tsukuba 305-0047, Japan*
[b]*Institute of Advanced Energy, Kyoto University, Uji 611-0011, Japan*

Received 30 April 2004; received in revised form 5 May 2004; accepted 28 June 2004
Available online 1 September 2004

**Abstract**

SiC/SiC composites with single pyrolytic carbon (PyC) interlayer generally show significant strength degradations in oxidation/irradiation environments due to the poor oxidation/irradiation resistance of the PyC interlayer. Incorporating SiC sub-layers in the PyC interlayer $(SiC\text{-}PyC)_n$ multilayers has been proved effective on improving the oxidation/irradiation resistance of the materials. However, it remains unclear whether such stiff SiC sub-layer will cause decrease of the mechanical properties of a SiC/SiC composite, especially for newly developed advanced Tyranno-SA fibers reinforced one. In this study, two plain-woven Tyranno-SA/SiC composites with designed fiber/matrix interlayers of 100 nm PyC and 50 nm PyC + 150 nm SiC + 50 nm PyC, respectively, were fabricated to investigate the effects of the stiff SiC sub-layer on the mechanical properties. The results showed that the SiC sub-layer caused much higher interfacial shear strength (ISS) in the composite. However, the two composites exhibited a similar level of proportional limit stress and ultimate flexural strength.


*Keywords:* B. Composites; C. Mechanical properties; D. SiC; Chemical vapor infiltration; PyC-SiC interlayers

## 1. Introduction

Ceramics possess many attractive properties for structural and non-structural applications at elevated temperatures and under severe environments. Yet, limited mechanisms for stress concentration alleviation, and hence catastrophic fracture behavior, largely limited their applications. The low fracture toughness of ceramics can be readily improved by the incorporation of reinforcement fibers, whiskers, and particles, etc. [1–3]. For continuous ceramic fiber reinforced ceramic matrix (CFCC) composites, such as SiC fibers reinforced SiC matrix composites (SiC/SiC), the fiber/matrix interface is critical on determining the performance of the materials [4–6]. A compliant interfacial layer(s) is necessary to produce modified reinforcement fibers/matrix interfacial bonding in a CFCC to allow interfacial debonding and matrix crack deflection/bridging by the fibers during the failure of the material. These energy-dissipating mechanisms provide for improved apparent fracture toughness and result in a non-catastrophic mode of failure. Carbon has been proved to be very effective interphase materials in CFCC [7]. SiC/SiC composites are very attractive for applications at high-temperature harsh environments. They are also expected to be used as structure materials in advanced nuclear fusion/fission plants [8]. However, SiC/SiC with carbon interlayer usually show significant degradation of performance when exposed to oxidation environment at elevated temperature [5] or under neutron irradiation [9] because of serious degradation/damage of the carbon interlayer under these conditions. Fortunately, it was found that when the carbon layer is thin enough (less than 100 nm), the oxidation of the carbon interphase could be limited due to a 'self-healing' behavior [5]. Improving the oxidation and irradiation resistance requires thinner carbon interlayer, while deviation of matrix cracks needs sufficient thickness of the interphase [7]. Therefore, an alternating multilayer $(PyC\text{-}SiC)_n$, with thin

* Corresponding author. Tel.: +81 298 59 2842; fax: +81 298 59 2701.
*E-mail address:* yang.wen@nims.go.jp (W. Yang).

0272-8842/$30.00 
doi:10.1016/j.ceramint.2004.06.018

but multiple PyC sub-layers, has been developed [5,10]. Improved oxidation resistance of several Hi-Nicalon fiber reinforced SiC/SiC composites with such multilayers have been reported [10,11].

Although SiC/SiC composites with $(PyC\text{-}SiC)_n$ multilayers showed promise of improving the oxidation resistance, it remains unclear whether such stiff SiC sub-layer in the multilayers will cause the degradation of the mechanical performances of the composites, especially for those reinforced with Tyranno-SA fiber, which is a newly developed advanced SiC fiber, with near stoichiometric C-Si chemistry and highly crystalline structure [12]. This fiber exhibits excellent mechanical properties, much improved thermal conductivity and thermal stability, and relatively low fabrication cost compared with the old-generation SiC-based fibers such as Nicalon-CG and Hi-Nicalom™ [8], although the Tyranno-SA fibers display lower failure strain (related to its high modulus), which limits the non-linear stress–strain domain of the SiC/SiC composites. The SiC/SiC composite reinforced with Tyranno-SA fibers also showed much higher statistic reliability of flexural strength [13]. Its Weibull modulus of strength upon three-point bending was 10.2 versus those of the Nicalon/SiC (2.1) and Hi-Nicalon/SiC (7.4) composites. Therefore, it is important issue to make an understanding of the effects of the carbon and/or $(PyC\text{-}SiC)_n$ interlayers on the interfacial properties and mechanical properties of the advanced Tyranno-SA/SiC composites.

Previous researches indicated that flexural strengths of Tyranno-SA/SiC composites were very sensitive to the thickness of carbon interlayer up to ~100 nm, beyond which no obvious change of the strength was observed [14]. In this study, two new Tyranno-SA/SiC composites with 100 nm PyC single-interlayer (TSA-SL) and 50 nm PyC + 150 nm SiC + 50 nm PyC multilayers (TSA-ML) were designed and fabricated to investigate the effects of the SiC sub-layer on the interfacial shear strength (ISS) and mechanical properties of the composites. Because of the limited number of specimens for each composite, only comparative three-point bending tests were performed for comparison with previous results.

## 2. Experimental

### 2.1. Interlayer deposition and composite fabrication

The composites were fabricated using a chemical vapor infiltration (CVI) system. Detailed process information can be found elsewhere [14]. In brief, two composite preforms were prepared with 2D plain-woven Tyranno-SA fiber cloths (as-received) in 0/90°. No surface pre-treatment was performed to the fibers. The volume loads of the fibers for both preforms were 43%. The preforms were densified with SiC matrix through thermal decomposition of $CH_3SiCl_3$ (MTS). MTS was carried by hydrogen with a volume ratio 1:10 and total hydrogen flow rate 1000 sccm. The preforms were kept at 1273 K during the CVI process. The matrix densification process continued for 17 h under reduced pressure (total reaction pressure) of 14.7 kPa. Prior to the matrix densification, fiber/matrix interfacial coatings with designed structures of 100 nm PyC and 50 nm PyC + 150 nm SiC + 50 nm PyC were deposited on the fiber surfaces in the two performs, respectively, using the same CVI system. $CH_4$ was used as source gas for PyC layer with processing conditions as: temperature, 1223 K; total pressure, 14.7 kPa; $CH_4$ flow rate, 200 sccm. The deposition conditions for the SiC sub-layer in the tri-interlayer composite were the same as the matrix densification. After the deposition of each sub-layer, the CVI system was maintained at the deposition temperatures for about 10 min to make sure a full reaction of the residual source gas in the furnace, then, moved to next sub-layer deposition.

Upon completing the fabrication process, the microstructure of the composites, the thickness and space uniformities of the deposited interlayers were inspected using scanning electron microscopy (SEM, JEOL JSM-6700F). The interlayer thickness was measured on high magnification SEM images from six areas over the cross-section of each composite with an estimated resolution of ~10 nm.

### 2.2. Mechanical tests

The mechanical properties and fracture behaviors were investigated by three-point bending tests (with a support span of 18 mm). Three tests were conducted for each composite. Specimens were cut parallel to one of the fiber bundle directions of the fabric cloth. Both the tensile and compression surfaces of each specimen were carefully ground using diamond slurry to eliminate the effects of surface CVD-SiC layers, which were formed at the end of the CVI process. The final dimension of the specimen was $L$30 mm × $W$4.0 mm × $T$1.5 mm. The crosshead speed was 0.0083 mm/s. The load/displacement data were recorded. Proportional limit stress (PLS) and ultimate flexural strength (UFS) were derived from the load/displacement curves according to ASTM C 1341-97 [15]. The fracture surfaces were observed with interfacial debonding and fiber pullouts using the SEM. Specimens that did not completely separate during the bending tests were carefully broken apart by hands so that the fracture surfaces could be examined.

As mentioned before, interfacial bonding strength is critical on determining the mechanical properties of SiC/SiC composites. Interfacial shear strength is associated with the fiber bond strength and represents the stress required to overcome the chemical bonding and static coefficient of friction between the fiber and the fiber coating [16]. The ISSs of both composites were investigated by single fiber pushout technique, which is a widely used technique for deriving ISS in SiC/SiC composites because of simplicity, easy in sample preparation, and relatively easy in obtaining

the most direct measurement of ISS [17–19]. The single fiber pushout tests were performed using a load controlled micro-indentation testing system with a Berkovich type diamond pyramidal indenter. The maximum load of the indenter is 0.88 N. Detailed description of the system and the experimental procedure can be found elsewhere [19]. The pushout specimens were cut from the composites with one of the fiber bundles perpendicular to the cut surfaces, and were carefully ground and polished at both surfaces with diamond paste to reduce the thickness of the specimens to ~50 μm. The final polish grain size was 1 μm. For each composite, 20 isolated fibers perpendicular to the polished surface were pushed out to extract the ISS, which was defined as

$$\mathrm{ISS} = \frac{F}{\pi D t} \quad (1)$$

where $F$ is the onset load for fiber pushout to occur, and $D$ and $t$ are the fiber diameter and specimen thickness, respectively.

## 3. Results and discussion

### 3.1. Density and interlayer structures of the composites

Fig. 1 shows the SEM images of the cross-section and pores distribution in composite TSA-SL, which shows that several relatively large inter-fiber bundle pores (a) were left in the matrix while the intra-fiber bundle area (b) was rather dense deposited. The relatively large inter-fiber bundle pores originated from the large pores at the intersections of crossed fiber bundles in the preform before the matrix densification. More fabrication process observations found that more appropriate arrangement between the fiber cloth layers in the preform would result in less and smaller inter-fiber bundle pores. The composite densities are as in Table 1. The average density of composite TSA-SL is 2.74 ± 0.02 mg/m$^3$ (corresponding to a porosity of ~10%), indicating quite dense and uniform matrix densification in the composite by the present CVI conditions. Composite TSA-ML showed a slightly lower density, 2.62 ± 0.03 mg/m$^3$.

Table 1
Composite densities and interphase structures

| Composite I.D. | Interphases (nm) | Density (mg/m$^3$) |
|---|---|---|
| TSA-SL | F/C$^{120\ \pm\ 21}$/M | 2.74 ± 0.02 |
| TSA-ML | F/C$^{58\ \pm\ 9}$/SiC$^{140\ \pm\ 25}$/C$^{50\ \pm\ 12}$/M | 2.62 ± 0.03 |

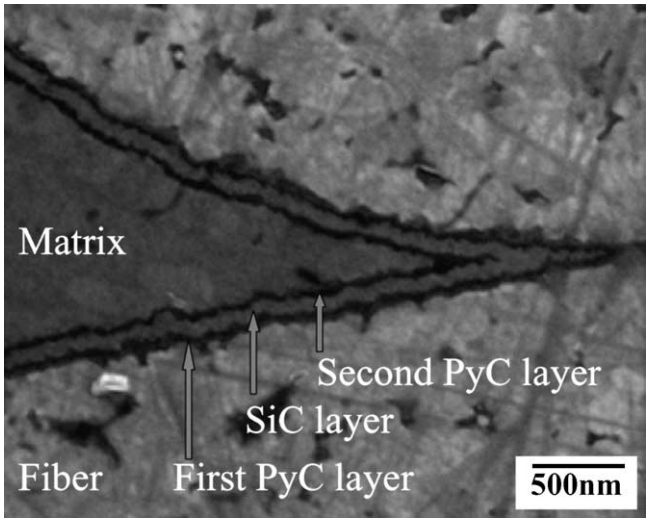


Fig. 2. The PyC + SiC + PyC tri-layer interphase structures in composite TSA-ML.

The interlayer structures and thickness were examined by high magnification SEM images. Fig. 2 shows the interlayer structure of composite TSA-ML, which clearly shows very thin PyC/SiC/PyC tri-layer interphase between the fiber and matrix in the composite. The measured thickness and standard deviations from six areas over the cross-section of both composite TSA-ML and TSA-SL are given in Table 1. The average thickness of the single PyC layer and PyC/SiC/

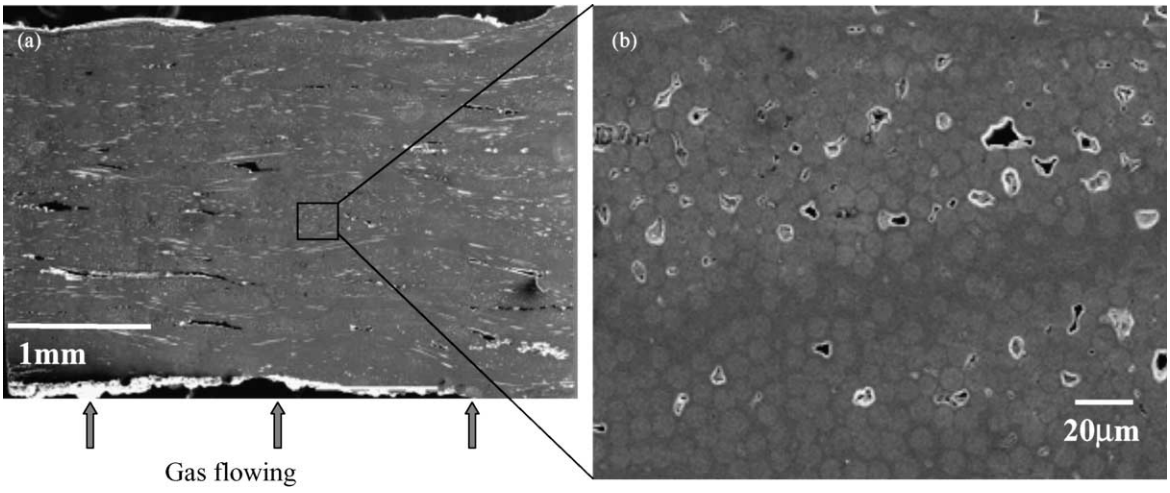


Fig. 1. Cross-section and inter/intra-fiber bundle pores in composite TSA-SL.

PyC tri-layer interphase are 120 and 58/140/50 nm, respectively, slightly deviated from the designed values (100 and 50/150/50 nm, respectively). The total amount of PyC in the two composites is almost the same, considering the estimated resolution (∼10 nm) of the measurement and the standard deviations of the thickness of each layer (Table 1). Table 1 and Fig. 2 show a successful deposition of either single PyC layer or thin PyC/SiC/PyC multilayers in the composites by the CVI process with quite fine thickness and space homogeneity control. The interfaces between the interphase layers (Fig. 2) in composite TSA-ML are fairly rough, apparently because of the grain growth in the SiC layer as well as the rough surface of the Tyranno-SA fiber. It is shown [20] that the morphology/surface roughness of CVD-SiC is closely dependent on the CVD conditions. Smoother SiC layer in present composite might be produced by optimization of the CVI conditions.

### 3.2. Mechanical properties and fracture behaviors

Representative load–displacement curves of the two composites are shown in Fig. 3. Both composites exhibited typical fracture behaviors for SiC/SiC upon bending loading: (1) an initial linear region, reflecting the elastic response of the composites, followed by (2) a non-linear domain of deformation until the load maximum, due mainly to the matrix cracking, interfacial debonding, and fiber sliding and pullouts, and individual fiber failures, (3) quick drop of the load after it reached its maximum, perhaps because of the failure of a significant fraction of the fibers. Certain downhill load is remained till large displacement depending mainly on the fraction of the remained intact fiber bundles in the specimen. These features are in accordance with the matrix cracking and fracture surface observations. For both composites, transverse matrix cracks initiated at the tensile surfaces of the specimens and propagated towards the compression surfaces with multiple deflections/deviations by the fiber bundles, as shown typically in the insert micrograph in Fig. 3. The fracture surfaces of both composites showed interfacial debonding and sound fiber pullouts fracture behaviors (Fig. 4(a)), owing to the deposited PyC or PyC/SiC/PyC interlayers. Fracture surface examinations revealed that the matrix cracks generally went through the interlayers and were deflected at the very fiber surfaces, independent on whether they were single PyC or PyC/SiC/PyC multilayers, as shown in high magnification SEM micrograph in Fig. 4(b), with bare fiber pullouts. Clearly, weaker bonding exists between the fiber surface and the first PyC-layer deposited from methane.

The average PLSs and UFSs of the two composites are summarized in Table 2. The average PLS and UFS of composite TSA-ML are 350 ± 53 and 520 ± 20 MPa, respectively, which are slightly lower than those of TSA-SL (370 ± 30 and 570 ± 26 MPa, respectively). As shown in Table 1, composite TSA-ML possesses a slightly lower density than TSA-SL, which might have negative effects on the strength. A statistic study [21] on the flexural strength of a CVI-Tyranno-SA/SiC composite showed that the flexural

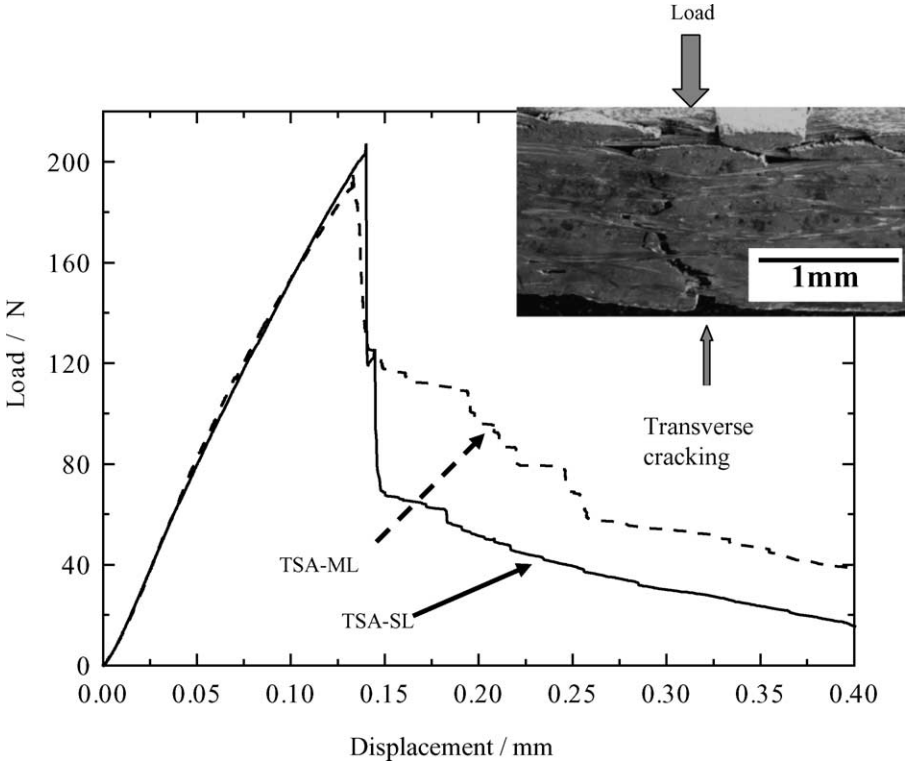


Fig. 3. Typical load–displacement curves of the composites.

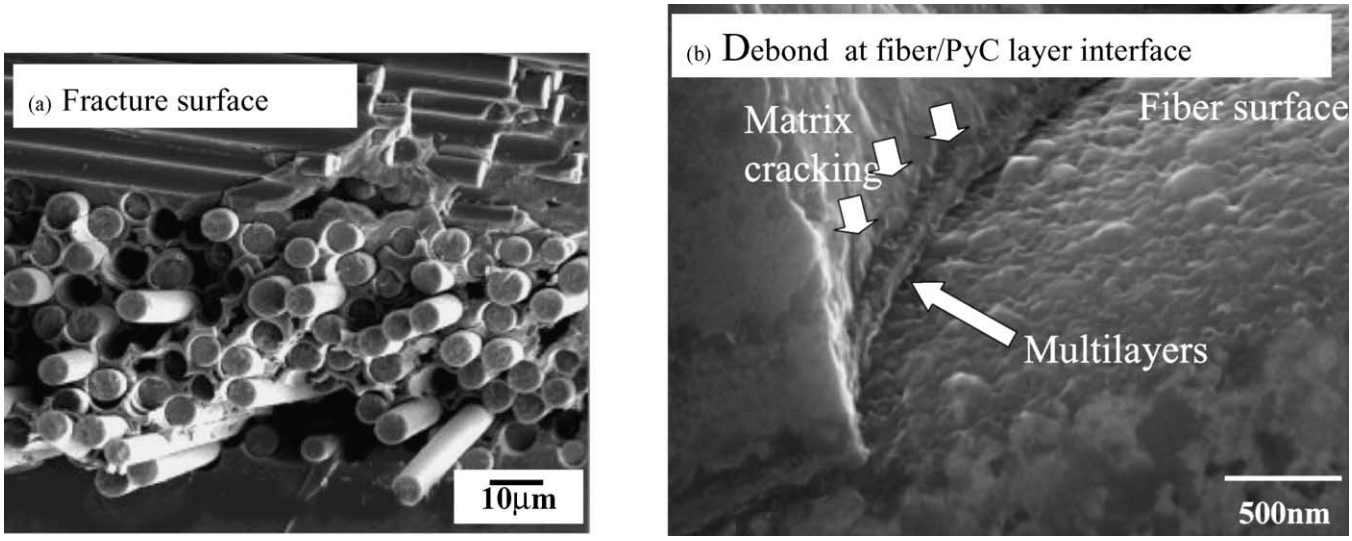


Fig. 4. SEM images of fracture surface of composite TSA-ML.

strength increased with higher specimen density. Here, by simply normalizing the strengths of present composites to densities, composites TSA-ML and SL showed similar level of both PLS and UFS, as shown in Table 2.

The obtained ISSs of the two composites are also given in Table 2. Composite TSA-ML exhibited an average ISS of 430 ± 165 MPa, much larger than that of TSA-SL, which is 300 ± 72 MPa.

### 3.3. Effects of SiC sub-layer on ISS

Generally, for given reinforcement fibers and process conditions for interlayer(s) and matrix, the ISSs of SiC/SiC composites are mainly determined by the amount of compliant (PyC) interlayer(s) [4–6,9]. The total PyC layer thickness in TSA-ML is ∼110 nm (Table 1), which is slightly less than that in TSA-SL (120 nm). Considering the resolution (∼10 nm) of the thickness measurements and the standard deviations of the interlayers, the difference in total PyC layer thickness between the two composites might be negligible. Both composites and interlayers were fabricated using the same CVI processes. Therefore, it is obvious that the increased ISS in TSA-ML is because of the incorporation of the sandwiched SiC sub-layer by the two PyC sub-layers. This becomes more evident when the ISS is graphically related to the PyC layer thickness, together with previous results [19] on investigating the effects of PyC layer thickness on the ISSs of several Tyranno-SA/PyC/SiC composites, as shown in Fig. 5 (the composites in Fig. 5 were fabricated using the same CVI process as in this study). Fig. 5 shows that the ISS of TSA-SL falls well into the trend of the PyC thickness dependence of the ISS, while the ISS of TSA-ML is obviously higher than those with single but similar total amount of PyC layer. When relating the ISS to the first PyC sub-layer (58 nm), the ISS showed much better fit to the PyC-ISS trend, as indicated by the dashed circle in Fig. 5. SEM examinations after the single fiber pushout tests revealed that the interfacial debondings and fiber pushouts predominantly occurred at the very fiber surfaces for both composites, as shown in Fig. 6 for TSA-ML, which shows that the fiber was pushed and popped while the PyC + SiC + PyC tri-layers remained within the matrix. Such interfacial debonding and fiber pushout behaviors indicate that the interfaces between fiber and PyC layer (for TSA-SL) and first PyC sub-layer (for TSA-ML) are the weakest link in the composites under single fiber pushout loading. From these observations, it is reasonable to assume that the PyC sub-

Table 2
The mechanical properties of the composites

| Composite | ISS (MPa) | PLS (MPa) | UFS (MPa) | PLS | UFS[a] |
|---|---|---|---|---|---|
| TSA-SL | 300 ± 72 | 370 ± 30 | 570 ± 26 | 140 ± 11 | 210 ± 9 |
| TSA-ML | 430 ± 165 | 350 ± 53 | 520 ± 20 | 140 ± 20 | 200 ± 7 |

[a] Normalized by composite densities (MPa/mg/m$^3$).

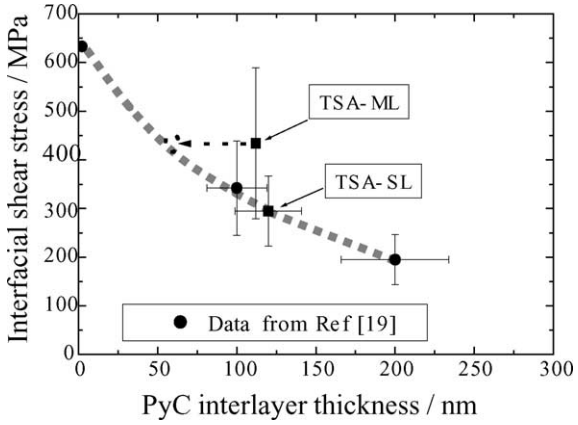


Fig. 5. PyC layer thickness dependence of the ISS of plain-woven Tyranno-SA/SiC composites.

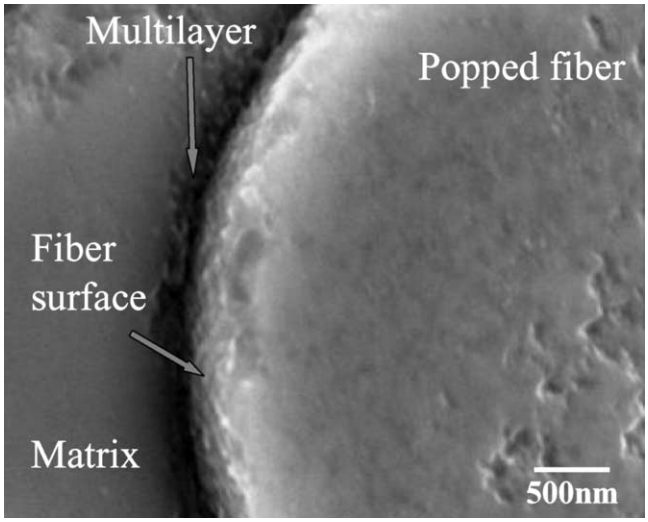


Fig. 6. The pushed and popped fiber in composite TSA-ML after pushout test (the multilayers remained in the matrix).

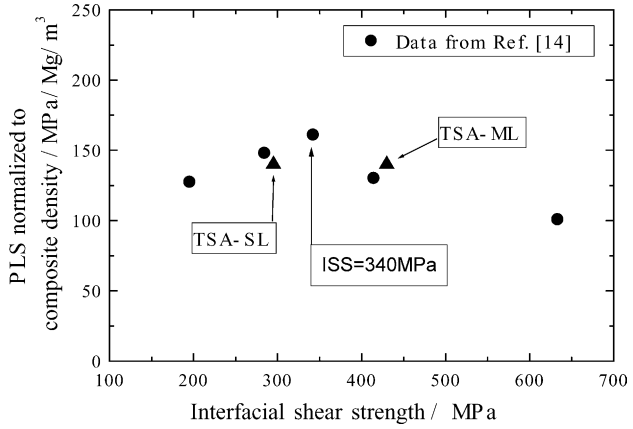


Fig. 7. Effects of ISS on PLS of plain-woven Tyranno-SA/SiC composites.

layer next to the fibers in TSA-ML affected the ISS of the material far larger than that of the PyC sub-layer next to the matrix. Similar experimental observation, the interfacial bonding strength seemed to be related to the thickness of the first carbon layer (nearest to the fibers) of Nicalon fiber reinforced CVI-SiC/SiC composites with $(C\text{-}SiC)_n$ interlayers, was reported by Rebillat et al. [7].

### 3.4. Effect of SiC sub-layer on flexural strength

Both theoretical and experimental studies [14,22,23] showed that ISS is a critical factor on determining the flexural strength of SiC/SiC composites. SiC/SiC composites with different ISSs generally show different flexural strengths. However, in this study, composite TSA-ML showed much higher ISS but yielded a similar level of flexural strength (PLS and UFS) to TSA-SL. This result seems contrary to already established knowledge. It was found [14] that for CVI-Tyranno-SA (plain-woven)/SiC composites, there exists an optimum ISS regarding the flexural strength (PLS and UFS). The strength increases with the increasing of the ISS up to the optimum value, beyond which the strength decreases gradually. A graphic illustration of the flexural strength of present composites against their ISSs might be able to get an easier understanding of present results. Fig. 7 relates the PLSs of several composites (the present two composites and those from ref. [14]) to their ISSs. All the PLSs in Fig. 7 were normalized to composite density to minimize the effect of composite density. The ISSs of the present two composites fall at either side of the optimum ISS (~340 MPa) and happened to obtain almost the same value of PLS, owing to the near symmetrical shape of the curve around 340 MPa of ISS. Similar situation occurred when relating the UFSs to ISS. Combining the effects of PyC and SiC layers on the ISS (Fig. 5), and the effects of ISS on PLS (Fig. 7) and UFS, this study indicates that the incorporation of SiC sub-layer in multilayered Tyranno-SA/SiC composites, such as fiber/PyC + SiC + PyC/matrix, may not cause a decrease of the mechanical properties, but depend on the value of ISS, which is largely determined by the thickness of the first PyC sub-layer. Similarly, Bertrand et al. [24] has found that the mechanical behaviors of unidirectional reinforced Hi-Nicalon/PyC/SiC and Hi-Nicalon/$(PyC\text{-}SiC)_n$/SiC composites upon tensile loading did not differ significantly except when the thickness of the PyC-layer became very low.

## 4. Conclusions

Two plain-woven Tyranno-SA/SiC composites with designed interlayers of 100 nm PyC and 50 nm PyC + 150 nm SiC + 50 nm PyC, respectively, were fabricated. High-magnification S.E.M. examinations of the interlayer structures and the thickness of each layer confirmed a successful deposition of the thin single and multilayers in the composites with quite well thickness and uniformity control toward the designed value by the CVI process.

Composite with PyC + SiC + PyC interlayers showed much larger ISS compared with that of composite with single PyC interlayer. The ISS of the multilayered Tyranno-SA/SiC composite is predominantly affected by the thickness of the first PyC sub-layer on the fiber, rather than the total and/or the second PyC sub-layer. The interfacial debonding and fiber pushouts occurred at the fiber/first PyC layer interface upon single fiber pushout loading.

The incorporation of stiff SiC sub-layer in multilayers did not cause noticeable change of the flexural strength of the present composite. However, this may not be always true. This study indicates that SiC sub-layer(s) in multilayered SiC/SiC composites may not cause a decrease of the mechanical strength, but depend on the value of ISS, which is largely determined by the thickness of the first PyC layer on the fibers.

## Acknowledgements

This work is supported by the CREST, Japan Science and Technology Corporation, and conducted at the National Institute for Materials Science. A part of this study was financially supported by the Budget for Nuclear Research of the Ministry of Education, Culture, Sports, Science and Technology, based on the screening and counseling by the Atomic Energy Commission.

## References

[1] A.G. Evans, Perspective on the development of high-toughness ceramics, J. Am. Ceram. Soc. 73 (1990) 187–206.
[2] K.M. Prewo, J.J. Brennan, Silicon carbide fiber reinforced glass-ceramic matrix composites exhibiting high strength and toughness, J. Mater. Sci. 17 (1982) 2371–2383.
[3] G.N. Morscher, J.D. Cawley, Intermediate temperature strength degradation in SiC/SiC composites, J. Eur. Ceram. Soc. 22 (14–15) (2002) 2777–2787.
[4] R.A. Lowden, Fiber coatings and the mechanical properties of a fiber-reinforced ceramic composite, Ceram. Trans. 19 (1991) 619–663.
[5] R. Naslain, The concept of layered interphases in SiC/SiC, Ceram. Trans. 58 (1995) 23–39.
[6] T.M. Besmann, D.P. Stinton, E.R. Kupp, S. Shanmugham, P.K. Liaw, Fiber–matrix interfaces in ceramic composites, J. Mater. Res. Soc. Symp. Proc. 458 (1997) 147–159.
[7] F. Rebillat, J. Lamon, R. Naslain, E. Lara-Curzio, M.K. Ferber, T.M. Besmann, Properties of multi-layered interphases in SiC/SiC chemical-vapor-infiltrated composites with 'weak' and 'strong' interfaces, J. Am. Ceram. Soc. 81 (1998) 2315–2326.
[8] A. Kohyama, M. Seki, K. Abe, T. Muroga, H. Matsui, S. Jitsukawa, S. Matsuda, Interactions between fusion materials R&D and other technologies, J. Nucl. Mater. 283–287 (2000) 20–27.
[9] T. Hinoki, L.L. Snead, Y. Katoh, A. Kohyama, R. Shinavski, The effect of neutron-irradiation on the shear properties of SiC/SiC composites with varied interface, J. Nucl. Mater. 283–287 (2000) 376–379.
[10] S. Bertrand, R. Pailler, J. Lamon, Influence of strong fiber/coating interfaces on the mechanical behavior and lifetime of Hi-Nicalon/(PyC/SiC)$_n$/SiC minicomposites, J. Am. Ceram. Soc. 84 (2001) 787–794.
[11] S. Pasquier, J. Lamon, R. Naslain, Tensile static fatigue of 2D SiC/SiC composites with multilayered (PyC-SiC)$_n$ interphases at high temperatures in oxidizing atmosphere, Comp. Part A 29A (1998) 1157–1164.
[12] T. Ishikawa, Y. Kohtoku, K. Kumagawa, T. Yamamura, T. Nagasawa, High-strength alkali-resistance sintered SiC fiber stable to 2200 °C, Nature 391 (1998) 773–775.
[13] W. Yang, H. Araki, A. Kohyama, C. Busabok, Q. Hu, H. Suzuki, T. Noda, Flexural strength of a plain-woven Tyranno-SA fiber-reinforced SiC matrix composite, Mater. Trans. 44 (2003) 1797–1801.
[14] W. Yang, T. Noda, H. Araki, J. Yu, A. Kohyama, Mechanical properties of several advanced Tyranno-SA fiber-reinforced CVI-SiC/SiC composites, Mater. Sci. Eng. A345 (2003) 28–35.
[15] ASTM C 1341-97, Standard test method for flexural properties of continuous fiber-reinforced advanced ceramic composites, 2000, pp. 509–526.
[16] E. Lara-Curzio, Properties of CVI-SiC matrix composites, in: Elsevier Comprehensive Composites Encyclopedia, 2000, pp. 533–577.
[17] D.B. Marshall, W.C. Oliver, Measurement of interfacial mechanical properties in fiber-reinforced ceramic composites, J. Am. Ceram. Soc. 70 (1987) 542–548.
[18] R.N. Singh, S.K. Reddy, Influence of residual stress, interface roughness, and fiber coatings on interfacial properties in ceramic composites, J. Am. Ceram. Soc. 79 (1996) 137–147.
[19] W. Yang, A. Kohyama, T. Noda, Y. Katoh, T. Hinoki, H. Araki, J. Yu, Interfacial characterization of CVI-SiC/SiC composites, J. Nucl. Mater. 307–311 (2002) 1088–1092.
[20] D. Lespiaux, F. Langlais, R. Naslain, A. Schamm, J. Sevely, Correlation between gas phase supersaturation, nucleation process and physico-chemical characteristics of silicon carbide deposited from Si–C–H–Cl system on silica substrate, J. Mater. Sci. 30 (1995) 1500–1510.
[21] H. Araki, T. Noda, W. Yang, Q-L. Hu, H. Suzuki, Flexural properties of several SiC fiber-reinforced CVI-SiC matrix composites, Ceram. Trans. 144 (2002) 281–287.
[22] E. Inghels, J. Lamon, An approach to the mechanical behavior of SiC/SiC and C/SiC ceramic matrix composites, part 1, experimental results, J. Mater. Sci. 26 (1991) 5403–5410.
[23] E. Inghels, J. Lamon, An approach to the mechanical behavior of SiC/SiC and C/SiC ceramic matrix composites, part 2, theoretical approach, J. Mater. Sci. 26 (1991) 5411–5419.
[24] S. Bertrand, P. Forio, R. Pailler, J. Lamon, Hi-Nicalon/SiC minicomposites with (pyrocarbon/SiC)$_n$ nanoscale multilayered interphases, J. Am. Ceram. Soc. 82 (1999) 2465–2473.